2007

Evidence for Inverted-Spectrum 20 GHz Emission in the Galactic Plane

Stephen P. Boughn
Haverford College, sboughn@haverford.edu

J. C. Pober '07
Class of 2007, Haverford College

Repository Citation

"Evidence for Inverted Spectrum 20 GHz Emission in the Galactic Plane" (with J. C. Pober), Ap. J. 661, 938 (2007).

The Astrophysical Journal, 661:938–943, 2007 June 1

EVIDENCE FOR INVERTED-SPECTRUM 20 GHz EMISSION IN THE GALACTIC PLANE

S. P. Boughn and J. C. Pober
Department of Astronomy, Haverford College, Haverford, PA 19041; sboughn@haverford.edu
Received 2006 November 14; accepted 2007 February 28

ABSTRACT

A comparison of a 19 GHz full-sky map with the *WMAP* satellite K-band (23 GHz) map indicates that the bulk of the 20 GHz emission within 7° of the Galactic plane has an inverted (rising) spectrum with an average spectral index $\alpha = 0.21 \pm 0.05$. While such a spectrum is inconsistent with steep-spectrum synchrotron ($\alpha \sim -0.7$) and flat-spectrum free-free ($\alpha \sim -0.1$) emission, it is consistent with various models of electric dipole emission from thermally excited spinning dust grains, as well as models of magnetic dipole emission from ferromagnetic dust grains. Several regions in the plane, e.g., near the Cygnus arm, have spectra with even larger α. While the low signal-to-noise ratio of the 19 GHz data precludes a detailed map of the spectral index, especially off the Galactic plane, it appears that the bulk of the emission in the plane is correlated with the morphology of dust. Regions with higher 23 GHz flux tend to have harder spectra. Off the plane, at Galactic latitudes $7^\circ < |b| < 20^\circ$, the spectrum steepens to $\alpha = -0.16 \pm 0.15$.

Subject headings: diffuse radiation — dust, extinction — Galaxy: disk — ISM: general — radiation mechanisms: thermal — radio continuum: ISM

1. INTRODUCTION

The spatial power spectrum of the cosmic microwave background (CMB) constitutes one of the most important observations in cosmology (Bennett et al. 2003a). In order to accurately measure the fluctuations in the CMB, it is essential to correct for diffuse Galactic emission; this need has led to a keen interest in microwave and far-infrared emission of the interstellar medium (ISM). Three known sources of emission, synchrotron, free-free (bremsstrahlung), and thermal dust emission (above 60 GHz), have all been identified in observations of the CMB (Bennett et al. 2003b). A decade ago, data from the *Cosmic Background Explorer* (*COBE*) satellite indicated that at least some of the microwave continuum below 60 GHz is spatially correlated with Galactic dust (Kogut et al. 1996a, 1996b). Both the magnitude and frequency dependence of this dust-correlated component are inconsistent with thermal dust emission, while low-frequency ($\lesssim$1 GHz) synchrotron emission is largely uncorrelated with dust. In addition, the lack of a strong correlation with Hα emission led Draine & Lazarian (1998a) to argue on energetic grounds against the possibility of the presence of dust-correlated free-free emission. They instead proposed the mechanism of electric dipole emission from thermally excited spinning dust grains (Draine & Lazarian 1998a, 1998b) and later that of magnetic dipole emission from ferromagnetic grains (Draine & Lazarian 1999). Since then, many observations have confirmed the presence of dust-correlated, low-frequency emission (de Oliveira-Costa et al. 1997, 1998, 1999, 2002; Leitch et al. 1997; Mukherjee et al. 2001, 2002), although some observations failed to detect this emission (de Oliveira-Costa et al. 2000; Hamilton & Ganga 2001; Mukherjee et al. 2003). The spinning dust spectrum is distinguished by a peak at $\sim$20 GHz, a spectral feature that has been tentatively identified in two specific sources (Finkbeiner et al. 2002) and in a survey of the Galactic plane (Finkbeiner et al. 2004), although subsequent observations of one of the former two sources, an H II region, have indicated that the emission is consistent with optically thin free-free emission with little contribution from spinning dust (Dickinson et al. 2006). In their analysis of *Wilkinson Microwave Anisotropy Probe* (*WMAP*) satellite data, Bennett et al. (2003b) suggested a model of "hard" synchrotron emission from supernovae remnants that is correlated with dust, but not with "soft" synchrotron emission at low frequencies ($\lesssim$1 GHz). While it is likely that hard synchrotron emission does contribute to 20 GHz emission in the Galactic plane, the rising spectrum reported by Finkbeiner et al. (2004) and in this paper requires a substantial contribution of another source with an even harder (inverted) spectrum.

2. METHOD

In this paper, we compare a full-sky 19 GHz map (Cottingham 1987; Boughn et al. 1992) with the three-year *WMAP* K and Ka-band maps (Hinshaw et al. 2006) in order to determine a spectral index in and near the Galactic plane. The *WMAP* 1° smoothed K- and Ka-band intensity maps were corrected for CMB fluctuations by subtracting the *WMAP* internal linear combination (ILC) CMB map and then convolved with the 19 GHz antenna beam pattern, including sidelobes out to 90°, to match the 3° angular resolution of the 19 GHz map. The dipole and CMB were similarly removed from the 19 GHz map, and all maps were converted to a common 24,576 $1.3^\circ \times 1.3^\circ$ pixelization in an equatorial quadrilateralized spherical cube projection on the sky (White & Stemwedel 1992). The mean instrument noise per pixel of the 19 GHz data is $\sim$2 mK, which is by far the dominant source of statistical noise. (The mean instrument noise per pixel in the K and Ka maps is $\sim$6 μK.) The calibration uncertainty of the K- and Ka-band data is 0.5% (Hinshaw et al. 2006), while that of the 19 GHz map is 3% (Boughn et al. 1992); however, the relative calibration of the two data sets is known to within 0.6%, the statistical accuracy with which the dipole in the 19 GHz map can be determined. By matching the dipoles of the data sets, all data were reduced to the same thermodynamic temperature scale.

Systematic errors are discussed in detail in § 4. One potential source of error is the unknown offset in the 19 GHz map. An estimate of this offset was determined by comparing the mean 19 GHz and K-band emissions at large Galactic latitudes ($30^\circ \le |b| \le 90^\circ$) and requiring the ratio of these two values to be consistent with a synchrotron spectrum. This conservative choice is discussed

TABLE 1
FITS FOR THE THERMODYNAMIC TEMPERATURE RATIO AND IMPLIED SPECTRAL INDEX

Latitude Bin (deg)	Bands	r	α	χ^2/ν	ν
0–7	19 GHz/K	1.327 ± 0.010	0.210 ± 0.048	1.244	2995
7–20	19 GHz/K	1.404 ± 0.032	−0.156 ± 0.148	1.067	5193
0–7	19 GHz/Ka	3.113 ± 0.023	−0.160 ± 0.014	1.335	2995
7–20	19 GHz/Ka	3.599 ± 0.082	−0.434 ± 0.043	1.077	5193

NOTES.—These fits are for r, the thermodynamic temperature ratio, and the implied spectral index, α, between 19 GHz and the K/Ka bands in two Galactic latitude bins, along with the reduced χ^2 and the number of degrees of freedom, ν, of the fits.

in § 4, along with possible variations of the offset with position in the sky. The offset uncertainty in the *WMAP* maps is on the order of ∼4 μK (Hinshaw et al. 2006) and is insignificant in the present analysis.

The ratio of the 19 GHz and K-band emission is then determined from a maximum likelihood (minimum χ^2) fit of this ratio times the K-band pixelized data to the 19 GHz data in the Galactic latitude region of interest where

$$\chi^2 = \sum_i (y_i - r x_i)^2/\sigma_i^2, \quad (1)$$

y_i is the 19 GHz flux in the ith pixel, x_i is the K-band flux, σ_i is the 19 GHz noise, and r is the presumed constant ratio of the 19 GHz to 23 GHz emission. There is a slight pixel-pixel correlation of instrument noise in the 19 GHz data, which we ignore. Its effect is small and, in any case, can be considered to be a systematic effect, as discussed in § 4.

3. RESULTS

Table 1 lists the fit values of the ratio of the 19 GHz to the K-band (23 GHz) and the Ka-band (33 GHz) data and the implied spectral indices in two different Galactic latitude bins. The quoted statistical errors are the 1 σ quadrature combination of instrument noise and calibration uncertainty. The transformation of the wideband K and Ka thermodynamic temperature data to the effective monochromatic Rayleigh-Jeans temperature necessary to compute the spectral index, α, was effected with the tabulated parameters in Jarosik et al. (2003). The 19 GHz data is narrowband, allowing the standard thermodynamic to Rayleigh-Jeans conversion to be used. Also listed in Table 1 are χ^2 and the number of degrees of freedom, ν, of the fits. Figure 1 is a plot of the 19 GHz and K-band thermodynamic temperatures for all 2996 pixels within 7° of the Galactic plane, along with the straight-line fit, the slope of which is the r listed in Table 1. Also shown in Figure 1 are dotted lines corresponding to α in the range −0.14 and −0.71, the spectral indices of free-free and soft synchrotron emission.

The scatter of the points in Figure 1 is dominated by 19 GHz instrument noise, and it is clear that most of the data points have low signal-to-noise ratio. This precludes a fine-scale map of α; however, averaging pixels on a larger angular scale does allow some measure of the variation of spectral index with position. Figure 2 is a plot of α derived from fits in individual $10^\circ \times 10^\circ$ regions centered at 5° intervals along the Galactic plane. While the errors on many of these points are quite large, there is significant variation of the spectral index along the Galactic plane within ±100° of the Galactic center, and there are several regions with α significantly larger than the value of 0.21 that characterizes the Galactic plane region as a whole. Of note is $\alpha \sim 0.77 \pm 0.13$ for the region centered on $\ell \sim 75^\circ$ near the Cygnus arm. As another more qualitative way to illustrate the variation

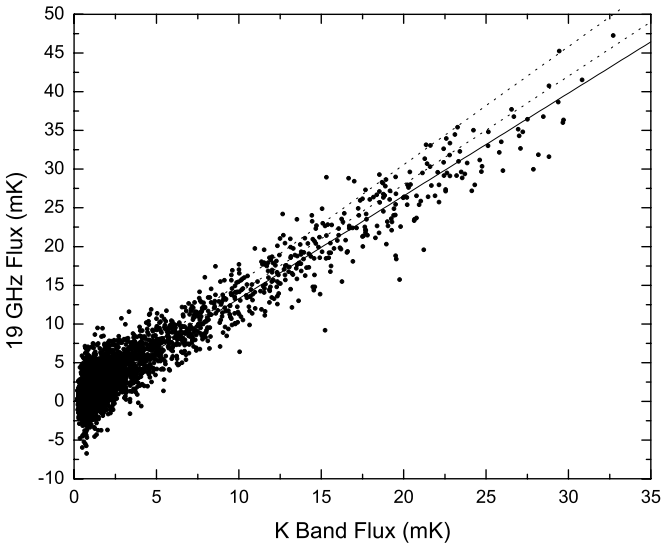

FIG. 1.—Correlation of 19 GHz emission with K-band emission for the 2996 pixels within 7° of the Galactic plane. The solid line shows the minimum χ^2 fit to the data, while the two dotted lines correspond to spectral indices of −0.14 (*smaller slope*) and −0.71 (*larger slope*) appropriate for free-free and soft synchrotron emission.

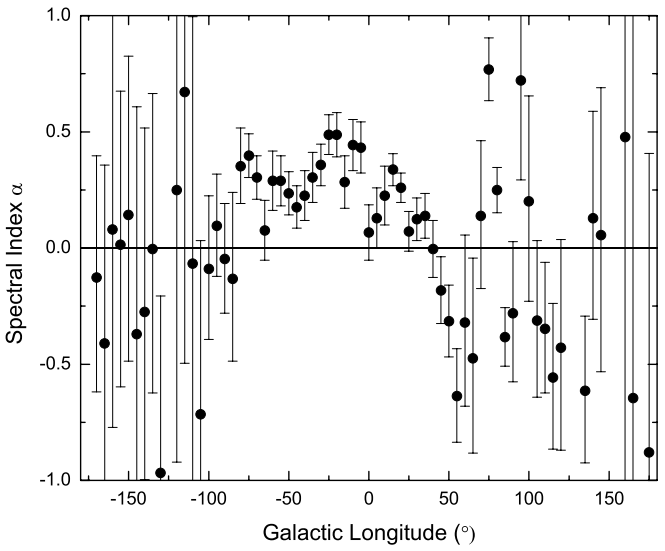

FIG. 2.—Mean spectral index, α, in $10^\circ \times 10^\circ$ regions at 5° intervals along the Galactic plane. The error bars represent statistical errors only.

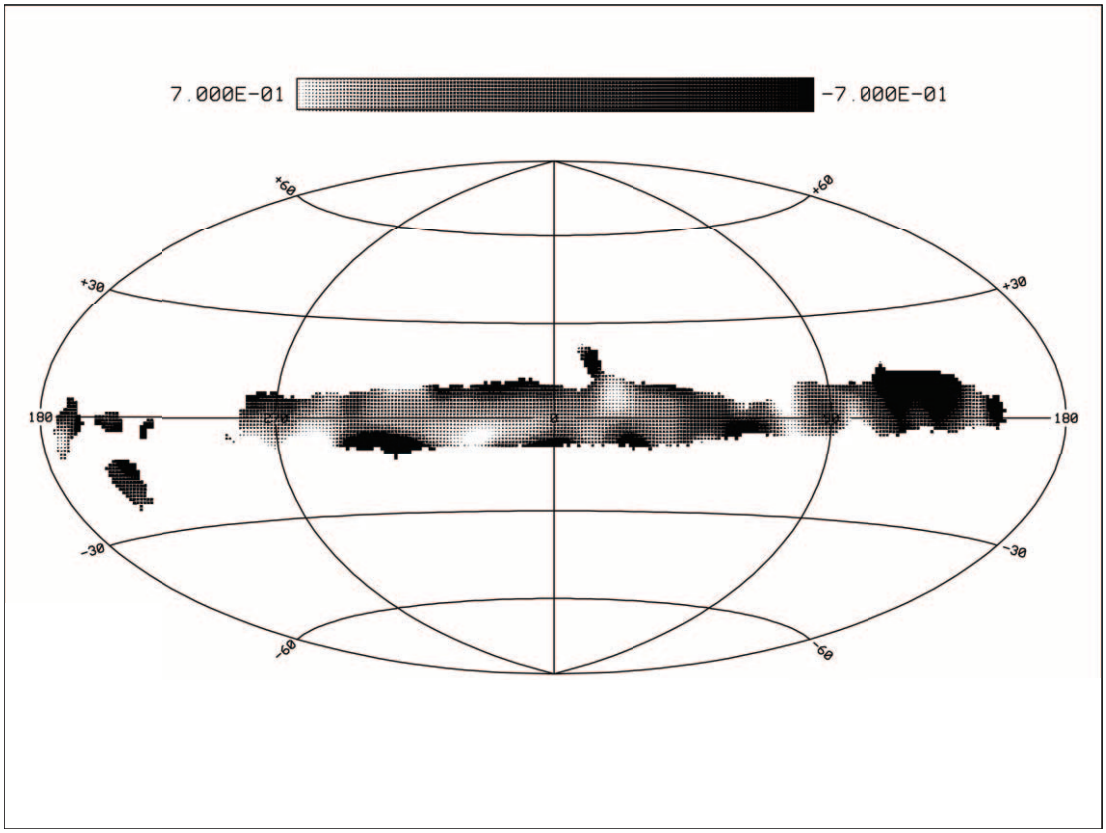

FIG. 3.—Map of the spectral index, $-0.7 < \alpha < 0.7$, deduced from the ratio of 19 GHz to K-band emission, smoothed to a resolution of 8° FWHM. Only those pixels for which the 19 GHz signal-to-noise ratio exceeds 10 are plotted.

of α, we smoothed the 19 GHz and K-band maps with an 8° FWHM Gaussian filter. Figure 3 is a map of α implied by the ratio of those pixels in the two maps for which the signal-to-noise ratio, $S/N = r/\sigma_r$, is greater than 10. The variations of α in Figure 3 are readily identified with corresponding regions in Figure 2.

So far we have not addressed the issue of whether the inverted-spectrum emission is associated morphologically with dust in the Galactic plane. A standard way to do this is to correlate a dust template with low-frequency emission. An effective spectral index for the dust-correlated component can be inferred from the relative amplitudes of the correlation at two different frequencies. Following Finkbeiner et al. (2004), we use the *WMAP* W-band (93 GHz) map, since "it is a good tracer of dust column density." The ratio of the linear minimum χ^2 fits of the W-band data to the 19 GHz and K-band data is then used to deduce an effective spectral index between 19 and 23 GHz. The 19 GHz σ_i values were used for the K-band data to ensure that the pixels in the two maps were weighted in the same way. The values deduced in this way differ insignificantly from those of Table 1, while the χ^2 are marginally worse, $\chi^2 = 1.442$ for the $|b| < 7°$ region and 1.093 for the $7° < |b| < 20°$ region. This suggests that the emission is, indeed, correlated with dust; however, it is also important to compare the results of fits to templates of other forms of emission, i.e., free-free and synchrotron. We take the 408 MHz map of Haslam et al. (1981) as a synchrotron template and the Hα map compiled by Finkbeiner (2003) and corrected for dust extinction by the *WMAP* team as a free-free template. The fits of these two templates to the 19 GHz data result in significantly worse χ^2 for the two regions, 6.15 and 1.18 for the synchrotron template fit and 11.85 and 1.30 for the free-free template fit. It should be pointed out that extinction corrections in the Galactic plane are only approximate; however, the corrected Hα map has structure similar to the *WMAP* MEM-derived free-free map (Bennett et al. 2003b) and so should provide a rough indication of the distribution of free-free emission. Also, the 408 MHz map is biased toward steep-spectrum, soft synchrotron emission and is unlikely to trace hard synchrotron emission. It is well known that the spectral index of synchrotron emission is harder (~ -0.5) toward the Galactic plane in regions of active star formation (Bennett et al. 2003b) and that this emission is correlated with dust. Therefore, dust-correlated emission includes both spinning dust and hard synchrotron emission.

For a direct comparison, we performed a three-parameter linear fit of the three templates, dust, free-free, and synchrotron, to the 19 GHz data. From the amplitudes of those fits, one can estimate the relative fraction of the 19 GHz emission that is associated with the three templates, as well as the spectral indices of the three sources of emission (by taking the ratio of the fit amplitudes to those of a fit to the K-band data). These values are listed in Table 2. The blank entries indicate relatively unconstrained α due to low emission. It should be noted that the χ^2 of the three-parameter fit in the $|b| < 7°$ region is only slightly lower than that of the fit to the dust template alone, which is consistent with the high estimated fraction of dust-correlated emission in that region. The χ^2 in the $7° < |b| < 20°$ region is marginally lower than that of the fit to the dust template alone and is also consistent with the relatively large fraction of estimated synchrotron emission. For comparison, the χ^2 of the 19 GHz data in the absence of any fit is 23.38 and 1.47 for the two latitude bins, an indication that the templates do, indeed, account for most of the morphology of the emission in the two regions. Even so, the χ^2

TABLE 2
Relative Fraction, f, and Spectral Index, α

Latitude Bin (deg)	Morphology	f	α	χ^2/ν
0–7	Dust	0.95	0.20 ± 0.08	1.422
	Free-free	0.03	...	
	Synch	0.02	...	
7–20	Dust	0.50	-0.05 ± 0.50	1.071
	Free-free	0.07	...	
	Synch	0.43	-0.60 ± 0.64	

Notes.—This table presents the relative fraction, f, of the contribution of different morphological types to 19 GHz emission and the associated spectral index α in two latitude bins.

in Table 2 indicate significant structure that is uncorrelated with the three templates. This is not unexpected, since the 19 GHz emission might well have a different dependence on physical parameters than do the templates. For this reason the relative fractions listed in Table 2 should not be taken too seriously. However, qualitatively, it seems reasonable to conclude that dust-correlated emission dominates in the plane, while dust and soft synchrotron–correlated emission are comparable off the plane. The latter is consistent with the off-plane α in Table 1. That the implied spectral index of the dust-correlated emission is larger than that of synchrotron-correlated emission in this region should be tempered by the large errors in these quantities.

4. SYSTEMATIC ERRORS

Systematic errors in the analysis fall in three main categories: relative pointing errors, differences in beam profiles, and offset errors. The pointing accuracy of the 19 GHz map is $\lesssim 1^\circ$ (Cottingham 1987). That the direction of the dipole in the 19 GHz data differs from that in the *WMAP* data by $0.7^\circ \pm 0.7^\circ$ is consistent with this estimate. The beam profile of the radiometer used to make the 19 GHz map is well approximated in the E-plane out to 90° and in the H-plane out to by 45° by the diffraction pattern of a TE_{11} mode launched from a circular waveguide (Boughn et al. 1990). The antenna was tipped 45° from the vertical in the H-plane, and radiation shields were employed to attenuate emission from the earth. This resulted in an additional attenuation of 20 db beyond $\approx 45^\circ$ in the forward H-plane, $\approx 90^\circ$ in the side E-planes, and $\approx 135^\circ$ in the back H-plane. The 60 db point occurred at 45° in the H-plane and 90° in the E-plane. The main beam is asymmetrical by about $\pm 13\%$ (Boughn et al. 1990), which results in a complicated and not easily modeled variation of angular resolution across the sky, because a given point on the sky is observed with more than one antenna orientation. An approximate beam pattern, consisting of an azimuthally averaged diffraction pattern cut off at 90°, was convolved with the *WMAP* maps. Changing the cutoff to 45° had a negligible effect on the analysis, so we conclude that the far sidelobe pattern has little effect on the results. The asymmetry of the main beam is relatively small compared to the angular resolution itself, and, furthermore, the values of α obtained are on even larger angular scales. However, to check for sensitivity to both pointing and beam asymmetry errors, we convolved both the 19 GHz and K-band maps with an additional 6° FWHM Gaussian. The fitted α-values for these maps were less by 0.98 and 0.55 σ than the values listed in Table 1 for the $|b| < 7^\circ$ and $7^\circ < |b| < 20^\circ$ regions, respectively. We also computed the spectral indices for the $10^\circ \times 10^\circ$ regions of Figure 2 by taking the ratio of the 19 GHz to K-band fluxes in these regions. This is equivalent to smoothing with a 11° FWHM filter. The α-values deduced this way differed, on average, from the values in Figure 2 by only 0.52 σ with regions of relatively low 19 GHz emission showing an increase in α and those regions with relatively high 19 GHz emission showing a decrease in α. Both of these small differences in spectral index are consistent with a spatial variation of α as discussed below; however, the general conclusion is that the systematic effects caused by errors in the beam profile and pointing do not significantly affect our analysis.

Another concern is the uncertainty in the value of the unknown offset in the 19 GHz data, as well as the uncertainty in the variation of the offset with position. It was pointed out above that there is a slight correlation in the noises of different pixels, which can result in a low-level systematic pattern in the map. This can be considered as simply contributing to a variable offset in the map. Our estimated constant offset, 0.15 mK, is that required to make the ratio of 19 to 23 GHz high-latitude ($|b| \geq 30^\circ$) emission consistent with a soft synchrotron spectrum, i.e., $\alpha \sim -0.7$. If high-latitude emission has a flatter spectrum, as would be the case for free-free or spinning dust emission, the implied offset would be larger. In turn, a larger offset would result in a larger α in our fits to the low Galactic latitude data. In this sense, the value of the offset we chose is conservative; however, even if the effective spectral index at high latitude were as large as in the plane, i.e., $\alpha \sim 0.2$, the implied offset would increase by only 0.03 mK and the implied α by only 0.014.

To investigate the large-scale variation in the offset, we computed it for separate hemispheres and separate quadrants of the sky, always in regions with Galactic latitude greater than 30°. The offsets deduced from the north, south, east, and west hemispheres and the northeast, northwest, southeast, and southwest quadrants have an rms difference from the nominal 0.15 mK of 0.025 mK, with a distribution consistent with instrument noise. Even if an offset gradient were this large, its effects would largely cancel out by symmetry in the above analysis of latitude bins. Of course, it might be possible that the offset near the plane is different than at large latitudes, i.e., a quadrupole effect. To check for this, we computed the offsets implied by the data in two different latitude bins, $30^\circ < |b| < 50^\circ$ and $50^\circ < |b| < 90^\circ$. These two offsets differed from our canonical value by 0.01 mK, about half the statistical error in the their determination. The statistical error of the canonical offset is 0.015 mK. Therefore, we find it unlikely that the error in the offset of the 19 GHz map is significantly larger than ~ 0.02 mK. For comparison, the statistical errors listed in Table 1 correspond to offset errors of 0.09 mK for the $|b| < 7^\circ$ bin and 0.03 mK for the $7^\circ < |b| < 20^\circ$ bin. We conclude that systematic error in the offset does not significantly change the results of Table 1.

One might choose to estimate an effective offset simply by including the offset as an additional free parameter in the minimum χ^2 fit of equation (1). Doing this for the data in the $|b| < 7^\circ$ region yields an offset of 0.38 ± 0.04 mK and a spectral index of $\alpha = 0.33 \pm 0.05$. The errors are somewhat larger than in Table 1, because of the correlation of the two parameters. The difference of this fit offset with our canonical value is roughly 5 times the statistical error. The discrepancy is likely due to the fact that α is not constant in the plane. It is apparent from Figure 2 that those regions with large K-band and 19 GHz fluxes, i.e., those with high signal-to-noise ratio, tend to have larger α than those with low fluxes. The third of the data points in the plane with the largest K-band fluxes have an average spectral index of $\langle \alpha \rangle = 0.27 \pm 0.02$, while the third with the lowest fluxes have $\langle \alpha \rangle = -0.63 \pm 0.15$ (statistical errors only). The same is true for the data of Figure 1. The third of the points with the

highest K-band fluxes have an average 19 GHz to K-band ratio of $r = 1.32$, corresponding to $\langle\alpha\rangle = 0.24 \pm 0.02$, while the third of the points with the lowest K-band fluxes have $r = 1.49$ and $\langle\alpha\rangle = -0.54 \pm 0.28$ (statistical errors only). The result of this variation is that the low K-band flux points in Figure 1 have elevated 19 GHz fluxes compared to those expected if the slope was that determined by the high K-band flux points. In a linear fit, this would appear as an additional offset of about the magnitude observed. We therefore conclude that our canonical offset determined at high Galactic latitudes is the appropriate choice. A two-parameter fit to the $7^\circ < |b| < 20^\circ$ data yields an offset within 0.02 mK of the nominal 0.15 mK and an α of -0.06, consistent with that listed in Table 1.

There is the possibility that anomalous small angular scale structure in the 19 GHz map, of the sort due to correlated noise, could affect the results expressed in Figures 2 and 3. To investigate this effect, we subtracted a scaled K-band map from the 19 GHz map and smoothed it with an 11° FWHM Gaussian filter (corresponding to the area of the bins in Fig. 2). A visual inspection of this map reveals the presence of systematic patterns even at high Galactic latitudes. The residual rms fluctuations (after correcting for instrument noise) at high latitudes, $|b| > 30^\circ$, is 0.12 mK. This should be considered an upper limit on systematic noise at this scale, since it is possible that there is still some contamination by real Galactic and extragalactic structure, as well as the possibility of a spatially varying spectral index between 19 and 23 GHz. For comparison, the statistical noise of the signals in the $10^\circ \times 10^\circ$ bins of Figure 2 correspond to effective offset errors in the range 0.17–0.45 mK, with an average of 0.27 mK. Therefore, the systematic offset errors are smaller than the errors quoted in Figure 2, and we conclude that it is unlikely that systematic errors can significantly change these results.

The χ^2 (see Table 1), of the fit of the K band to the 19 GHz data in the Galactic plane, $\chi^2 = 1.244$, while significantly different from unity, is not unexpected. The unaccounted-for (i.e., not due to instrument noise) rms residuals in the 19 GHz data are equivalent to an average of 0.78 mK per pixel. Some portion of the residuals is undoubtedly due to small-scale systematic structure in the map. This structure was estimated to be at the level of 0.12 mK when averaged over 100 deg^2 ($\sim$60 pixels), and on the scale of 1 pixel it will likely be larger. Pointing errors might also contribute to the residuals; however, the largest contribution is most likely due to the variation of α with position, as illustrated in Figures 2 and 3; that is, constant α is not the best model. If this is the case, then one would expect a larger such effect in the comparison of the 19 and 33 GHz maps. That the χ^2 of the 19 GHz to Ka-band fit in Table 1 ($\chi^2 = 1.350$) is significantly larger is in agreement with this expectation. The χ^2 of the fit in the $7^\circ < |b| < 20^\circ$ region is significantly smaller and corresponds to residual structure at the $\sim$0.39 mK per pixel level. So while the excessive values of χ^2 in Table 1 might temper our conclusions somewhat, they are not unexpected, and, in any case, the presence of the relatively small residuals in the fits does not change the conclusions of this paper.

5. DISCUSSION

The frequencies of the two data sets treated in this work are similar, 19.2 and 22.7 GHz. The ratio of the fluxes at the two frequencies, measured in units of thermodynamic temperature, is only 6% less than the expected ratio for free-free emission and 15% less than the expected ratio for soft synchrotron emission. However, the CMB dipole can be measured quite accurately at both frequencies, and consequently, the relative calibrations of the two data sets can be determined to within 0.6%, which is sufficient to distinguish between synchrotron, free-free, and spinning dust emission mechanisms. It is clear that 20 GHz emission in the Galactic plane is inconsistent with a combination of synchrotron and free-free emission alone and must include a significant component of inverted-spectrum emission, such as that due to spinning dust. Consider, for example, emission consisting of spinning dust with a spectral index of $\alpha = 1.0$ and hard synchrotron emission with spectral index $\alpha = -0.5$. The spectral index of emission consisting of equal amounts of these two components is $\alpha = 0.2$, the value determined for the Galactic plane in Table 1. Therefore, our results are consistent with spinning dust accounting for a significant fraction of the 20 GHz emission in the Galactic plane. This conclusion is strengthened by our finding that the morphology of the emission is much more correlated with dust than with the expected morphologies of soft synchrotron and free-free emission. From fits to templates of these three sources, we estimate that the 19 GHz emission within 7° of the Galactic plane is dominated by emission correlated with dust. To be sure, there is significant variation of the spectral index, as is indicated in Figures 2 and 3, including regions in which the spectral index is significantly less than zero. Finally, we find some evidence that regions of relatively high K-band flux have harder spectra than those with relatively low flux. This is also consistent with the fact that K-band and 19 GHz flux is relatively highly correlated with dust, which would have a hard spectrum due to the spinning dust mechanism.

We have only determined the average flux and spectral index of the emission near one frequency (20 GHz) and therefore have not attempted to fit the data to any particular model of spinning dust emission. Such models have many free parameters, e.g., grain size, composition, temperature, electric dipole moment, gas density, ionization fraction, etc. Suffice it to say that some models do have inverted 20 GHz spectra like those we observe, and the parameters can be adjusted to account for the level of emission (Draine & Lazarian 1998a). The rising spectrum detected from 19 to 23 GHz is in mild conflict with two of the four Galactic plane regions investigated by Finkbeiner et al. (2004). Although their analysis also supports the case for spinning dust emission, in these two regions (those centered at $\ell = 15^\circ$ and 30°) they detect a falling spectrum from 14 to 23 GHz. However, the quoted error is relatively large, and a somewhat lower 14 GHz flux would be consistent with the data in Figure 2. Their results in the other two regions, $\ell = 0^\circ$ and 45°, the former of which has a rising spectrum and the latter a falling spectrum, agree qualitatively with Figure 2. Finally, the effective spectral index between 19 and 33 GHz, the *WMAP* Ka band, is $\alpha \sim -0.16$ in the plane and $\alpha \sim -0.43$ in the $7^\circ < |b| < 20^\circ$ region. This observation is not necessarily inconsistent with spinning dust emission, the spectra of which can turn over at frequencies above 20 GHz.

We are grateful to Lyman Page,who suggested the comparison of the 19 GHz and K-band maps, and to Bruce Partridge for helpful conversations. Dave Cottingham constructed the 19 GHz map with the help of Ed Cheng and Dale Fixsen. We acknowledge the use of the Legacy Archive for Microwave Background Data Analysis (LAMBDA). Support for LAMBDA is provided by the NASA Office of Space Science.

REFERENCES

Bennnett, C. L., et al. 2003a, ApJS, 148, 1
———. 2003b, ApJS, 148, 97
Boughn, S. P., Cheng, E. S., Cottingham, D. A., & Fixsen, D. J. 1990, Rev. Sci. Instrum., 61, 158
———. 1992, ApJ, 391, L49
Cottingham, D. A. 1987, Ph.D. thesis, Princeton Univ
de Oliveira-Costa, A., Kogut, A., Devlin, M. J., Netterfield, C. B., Page, L. A., & Wollack, E. J. 1997, ApJ, 482, L17
de Oliveira-Costa, A., Tegmark, M., Gutiérrez, C. M., Jones, A. W., Davies, R. D., Lasenby, A. N., Rebolo, R., & Watson, R. A. 1999, ApJ, 527, L9
de Oliveira-Costa, A., Tegmark, M., Page, L. A., & Boughn, S. P. 1998, ApJ, 509, L9
de Oliveira-Costa, A., et al. 2000, ApJ, 542, L5
———. 2002, ApJ, 567, 363
Dickinson, C., Casassus, S., Pineda, J. L., Pearson, T. J., Readhead, A. C. S., & Davies, R. D. 2006, ApJ, 643, L111
Draine, B. T., & Lazarian, A. 1998a, ApJ, 494, L19
———. 1998b, ApJ, 508, 157
———. 1999, ApJ, 512, 740
Finkbeiner, D. P. 2003, ApJS, 146, 407
Finkbeiner, D. P., Langston, G. I., & Minter, A. H. 2004, ApJ, 617, 350
Finkbeiner, D. P., Schlegel, D. J., Frank, C., & Heiles, C. 2002, ApJ, 566, 898
Hamilton, J. C., & Ganga, K. M. 2001, A&A, 368, 760
Haslam, C. G. T., Klein, U., Salter, C. J., Stoffel, H., Wilson, W. E., Cleary, M. N., Cooke, D. J., & Thomasson, P. 1981, A&A, 100, 209
Hinshaw, G., et al. 2006, ApJ, submitted (astro-ph/0603451)
Jarosik, N., et al. 2003, ApJS, 145, 413
Kogut, A., Banday, A. J., Bennett, C. L. Górski, K. M., Hinshaw, G., & Reach, W. T. 1996a, ApJ, 460, 1
Kogut, A., Banday, A. J., Bennett, C. L. Górski, K. M., Hinshaw, G., Smoot, G. F., & Wright, E. L. 1996b, ApJ, 464, L5
Leitch, E. M., Readhead, A. C. S., Pearson, T. J., & Myers, S. T. 1997, ApJ, 486, L23
Mukherjee, P., Coble, K., Dragovan, M., Ganga, K., Kovac, J., Ratra, B., & Souradeep, T. 2003, ApJ, 592, 692
Mukherjee, P., Dennison, B., Ratra, B., Simonetti, J. H., Ganga, K., & Hamilton, J. C. 2002, ApJ, 579, 83
Mukherjee, P., Jones, A. W., Kneissl, R., & Lasenby, A. N. 2001, MNRAS, 320, 224
White, R. A., & Stemwedel, S. W. 1992, in ASP Conf. Ser. 25, Astronomical Data Analysis Software and Systems I, ed. D. M. Worral, C. Biemesderfer, & J. Barnes (San Francisco: ASP), 379